ELSEVIER

Journal of Materials Processing Technology 84 (1998) 149–158

Journal of Materials Processing Technology

Effect of ultraprecision grinding on the microstructural change in silicon monocrystals

I. Zarudi, L.C. Zhang *

Centre for Advanced Materials Technology, Department of Mechanical and Mechatronic Engineering, The University of Sydney, Sydney NSW 2006, Australia

Received 25 May 1997

Abstract

The effect of ultraprecision grinding on microstructural change in silicon monocrystals, such as surface roughness and dislocation structure, was investigated both experimentally and theoretically. The study found that there exists an additional concentration of oxygen and carbon in an amorphous layer for all investigated grinding regimes with their distributions dependent on the grinding variables. It showed that two atomic bonding configurations exist in the amorphous layer, i.e. silicon oxide in the surface region followed by amorphous silicon. The research established that the grinding table speed affects the thickness of the dislocation layer in the subsurface. Increase of the table speed leads to a thicker dislocation zone and created microcracks. The paper concludes that the ductile mode of material removal in the grinding of silicon monocrystals is due to the formation of the amorphous phase.

Keywords: Ultraprecision grinding; Subsurface structure; Amorphous; Silicon

1. Introduction

The wide applications of silicon monocrystals in electronic devises demand that the machined surfaces of silicon components should be damage-free. However, traditional treatment such as ordinary grinding [1,2] normally introduces a severely deformed layer with cracks in the subsurface of a component, which then has to be removed in the subsequent finishing operations. Ultraprecision turning can produce a high surface quality [3] but microcracks, causing degradation of the turned components [4,5], are difficult to avoid.

A characteristic of the subsurface of a component machined by an ultraprecision process is that an amorphous surface layer normally appears, followed by a zone with a high density of dislocations and defects [2–5]. However, the origin of generation and the composition of the amorphous layer have not been understood well. The relationship between the microstructural change and processing conditions has not been developed. The present paper aims to gain an understanding of the subsurface damage of silicon monocrystals in terms of grinding conditions.

2. Experimental procedure

The {100} surfaces of silicon monocrystals were ground in the $\langle \bar{1}10 \rangle$ direction with an ultraprecision grinder Minini Junior 90 CF CNC M286[1], the grinding parameters used being listed in Tables 1–3.The properties of the ground surfaces were explored using a high resolution scanning electron microscope (HRSEM) JSM-6000F and an atomic force microscope (AFM). The subsurface structures were studied using a transmission electron microscope (TEM) EM 430 and scanning transmission electron microscope (STEM) VG HB601. At the same time, energy dispersive spectroscopy (EDS) was used to investigate the chemical compositions of the interested subsurface layers. To

* Corresponding author. Fax: +61 2 93513760; e-mail: zhang@mech.eng.usyd.edu.au

[1] A detailed explanation of the notations for slip systems and slip directions is given in Appendix A.

0924-0136/98/$ - see front matter
PII S0924-0136(98)00090-9

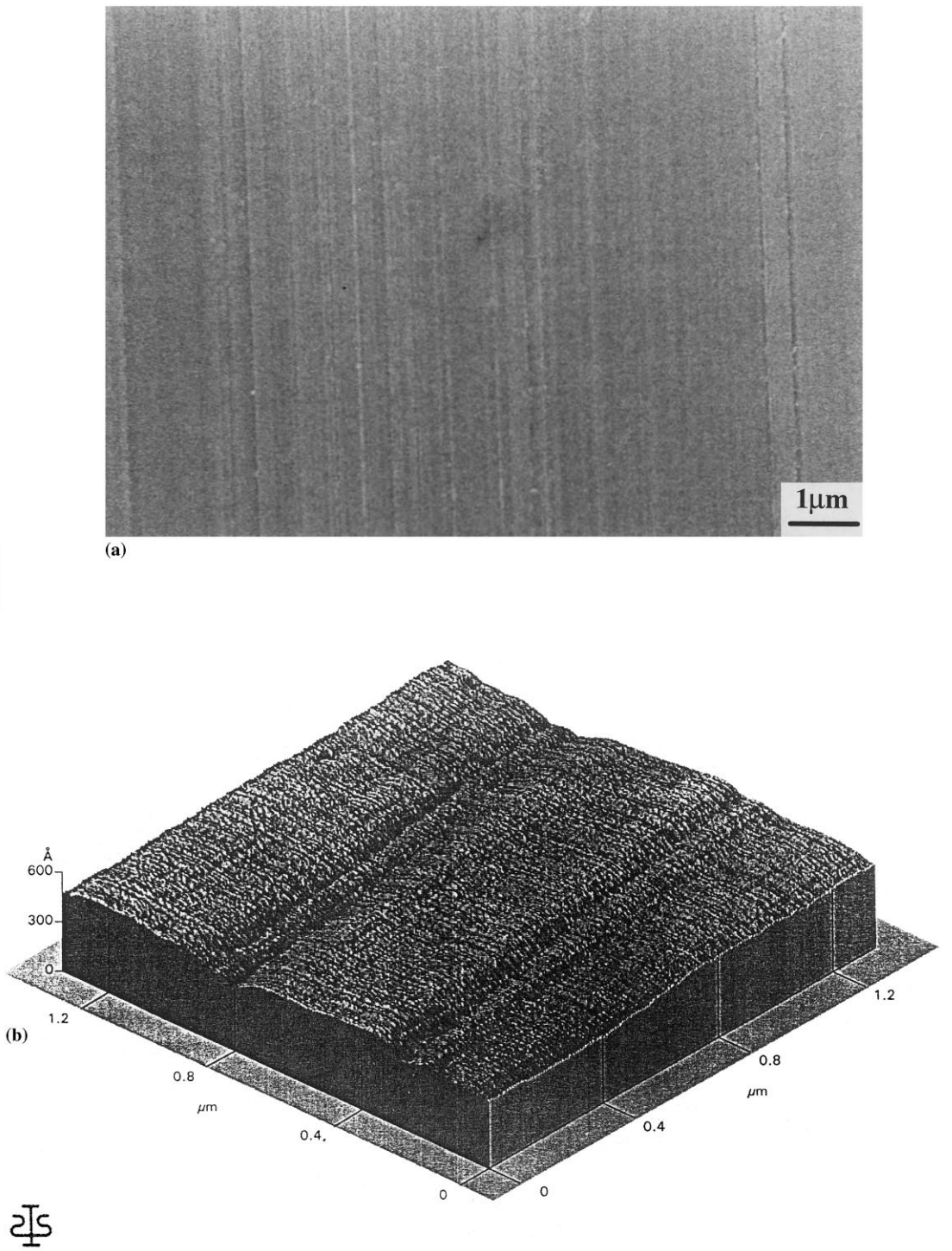

Fig. 1. Microtopography of ground silicon monocrystals, ground with a table speed of 0.02 m min^{-1}: (a) general view; and (b) 3-D image of a ground surface.

ensure the reliability of the examination results, at least five passes were conducted in analysing each specimen. On the other hand, to evaluate the atomic bonding in the deformed layer, electron energy loss spectroscopy (EELS) with a 1-nm probe diameter was employed. Cross-section view samples were made by the method presented in [6], whilst plan view samples were prepared by mechanical thinning and then ion milling of the side opposite to the ground surface. All of the preparations were carried out at room temperature.

Table 1
Grinding conditions

Workpiece material	Monocrystal Si wafers
Grinding wheel	SD4000L75BPF
Wheel diameter (mm)	305
Wheel speed (m min^{-1})	27
Grinding width (mm)	5
Table speed (m min^{-1})	0.02, 0.1, 0.2, 0.5, 1
Depth of cut (nm)	100
Coolant	Syntilo 3 (99% water, 1% mineral oil)

Table 2
Wheel dressing conditions

Type of dresser	Multipoint diamond
Wheel speed (m min^{-1})	10
Dressing, cross-feed rate (mm rev^{-1})	0.01

Table 3
Wheel truing conditions

Truing procedure	Feeding of a pyrex lap
Diameter of diamond abrasive in paste (μm)	6
Wheel speed (m min^{-1})	5
Truing cross-feed rate (mm rev^{-1})	0.01

Table 4
Variation of surface roughness of ground components with table speed

Table speed (m min^{-1})	1	0.5	0.2	0.1	0.02
Rms roughness (nm)	30	40	28	40	25
Deviation (nm)	6	6	6	6	6

3. Results and discussion

3.1. Ground surface

The surface topography of the ground Si is shown in Fig. 1. Mirror-like, microcrack- and pits-free surfaces were obtained with all the table speeds listed in Table 1. However, microgrooves were shown clearly (Fig. 1(b)), these demonstrating that the material removal had been fracture-free. Table 4 shows that the effect of the table speed on the surface roughness is not considerable.

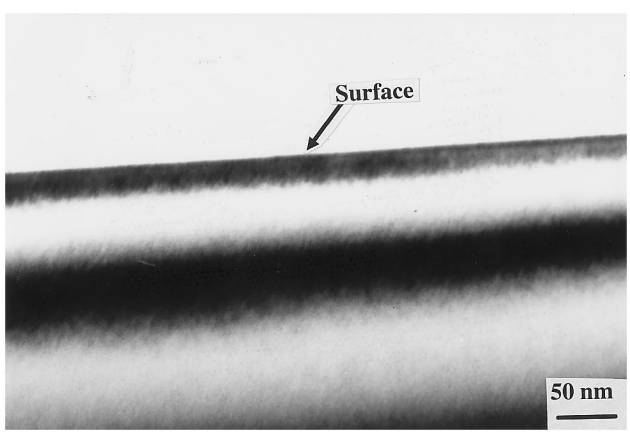

Fig. 2. Subsurface structure in a silicon monocrystal before grinding (polishing conditions according to Ref. [1]).

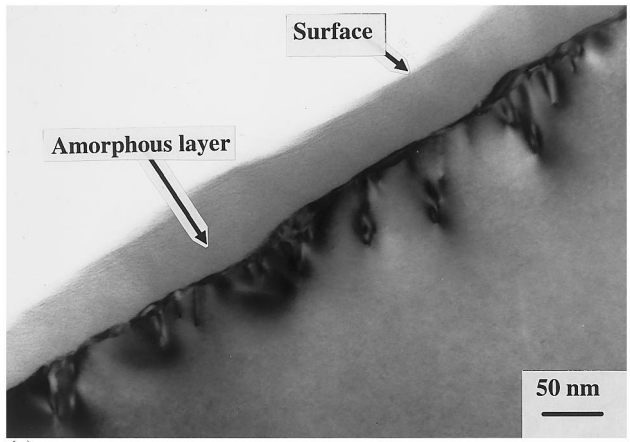

(a)

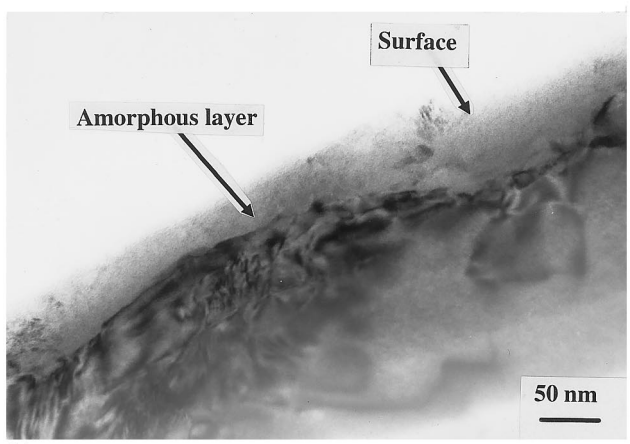

(b)

Fig. 3. Subsurface structure versus different table speed: (a) 0.02 m min^{-1}; and (b) 1 m min^{-1}.

3.2. Subsurface structure

The subsurface structure of specimens before grinding was damage-free (Fig. 2), which means that any microstructural changes detected thereafter must be caused by grinding.

3.2.1. The amorphous layer

The subsurface structure of a ground silicon shown in Fig. 3 presents two distinct regions and is common to all the specimens ground with five different table speeds. Diffraction analysis of plan view specimens showed that the top region has an amorphous structure

Table 5
Variation of the amorphous layer thickness with table speed

Table speed (m min^{-1})	1	0.5	0.2	0.1	0.02
Thickness of amorphous layer (nm)	60	53	48	42	36
Deviation (nm)	15	15	15	15	15

without any crystalline particles. Measurement using the transmission electron microscope showed that the thickness of the amorphous layer was not uniform with its average varying with table speed (Table 5). Increasing the table speed resulting in an increase in the thickness of the amorphous layer.

The main feature presented by the EDS spectrum of the amorphous layer (Fig. 4) is the peaks corresponding to carbon, oxygen and silicon. EDS linescans across the amorphous layer show the variation of concentration of elements C and O (Fig. 5), there being an increase in the concentration of both C and O across the whole thickness of the amorphous layer. The relative concentration of oxygen relative to that of silicon (Fig. 6) varies from about 70 at.% on the surface to almost zero at the bottom for all table speeds. However, Fig. 6 shows that the oxygen penetration is enhanced by an increase of table speed and is very different from that in polished components: in the latter the penetration depth is only about 5 nm and the highest concentration is about 50 at.%. It is therefore clear that the enhancement of oxygen penetration in grinding has a close relationship to its high speed abrasion. Similarly, carbon penetration in the subsurface of a ground component also increases with an increase in the table speed. However, it is difficult to evaluate the carbon concentration accurately due to many artificial factors involved.

EELS spectra of the amorphous layer in Fig. 7 indicates that there are two bonding configurations of silicon, silicon oxide and pure amorphous silicon. The silicon oxide, featuring a Si L-edge at 103 eV (Fig. 7(a)), appears immediately under the ground surface and spreads to approximately the two-thirds of the layer. The pure amorphous silicon then follows (Fig. 7(b)) with a Si L-edge at 98 eV. In addition to the L-edge positions, the shapes of the two spectres are also different and fit exactly the corresponding etalon spectres. On the other hand, modeling of nano-indentation processes of silicon monocrystals in vacuum has established that the formation of the amorphous layer can be the result of a pure phase transformation [7].

Based on all of the above observations and discussions, the formation mechanism of the amorphous layer in a ground component can be interpreted as follows. The abrasion results in amorphous phase transformation and the high speed impact between the abrasives and work material enhances the penetration of oxygen. When the oxygen concentration in the amorphous layer exceeds 45 at.%, SiO_2 forms due to the high affinity of oxygen for silicon: otherwise a pure amorphous silicon stays.

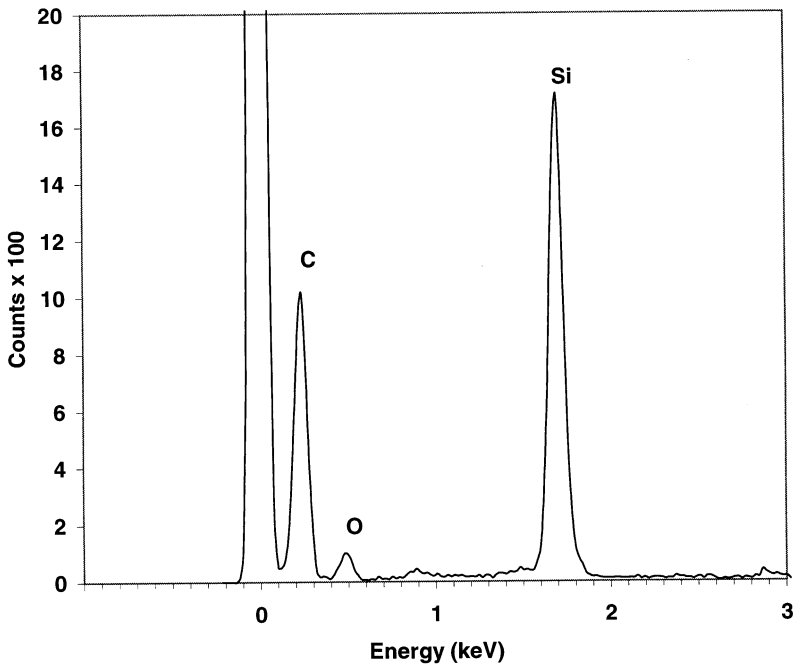

Fig. 4. Energy dispersive spectra of an amorphous layer, ground with A table speed of 1 m min^{-1}.

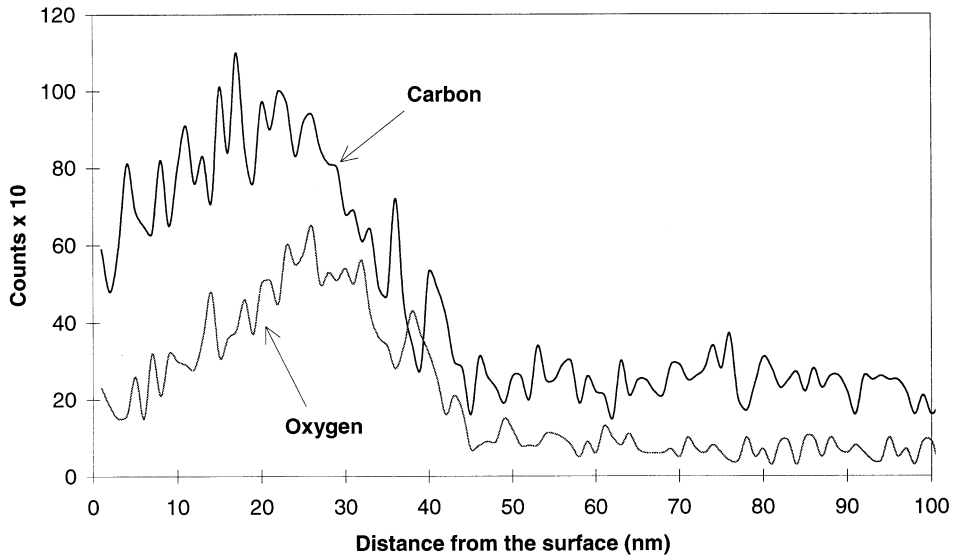

Fig. 5. Distribution of oxygen and carbon in the amorphous layer, ground with A table speed of 1 m min^{-1}.

3.2.2. Dislocations

Dislocations appear in the subsurface zone beneath the amorphous layer (Fig. 8), with their structure being highly dependent on the variation of table speed, the density of dislocations becoming high when table speed increases. For the case with a low table speed (0.02 m min^{-1}), individual dislocations with a penetration depth of between 100 and 200 nm under the amorphous layer can be distinguished easily (Fig. 8(a)). In this case only one slip system (111)[10$\bar{1}$] is generated (the grinding direction was [$\bar{1}$10]). With increase of the table speed both the density and penetration depth of dislocations increase. At a high table speed of 1 m min^{-1} (Fig. 8(b)), which was the highest speed used in this study, the dislocations penetrated from 300 to 600 nm, although non-uniformly. In this case two slip systems, (1$\bar{1}$1)[10$\bar{1}$] and (1$\bar{1}$1)[0$\bar{1}\bar{1}$], were activated (Fig. 8(b)).

3.2.3. Microcracks

Microcracks appeared only below the amorphous layer when the table speed reached 1 m min^{-1} (Fig. 8(c)). Thus, the initiation of microcracks is clearly

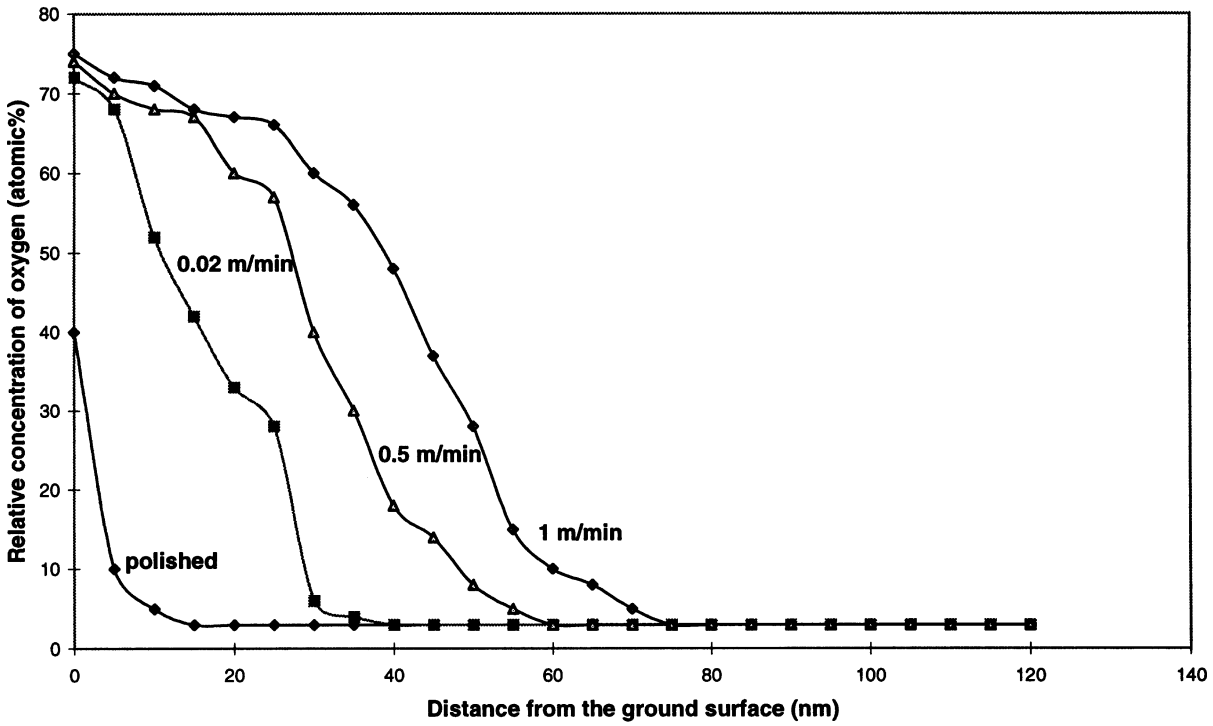

Fig. 6. Effect of table speed on the distribution of oxygen in the amorphous layer.

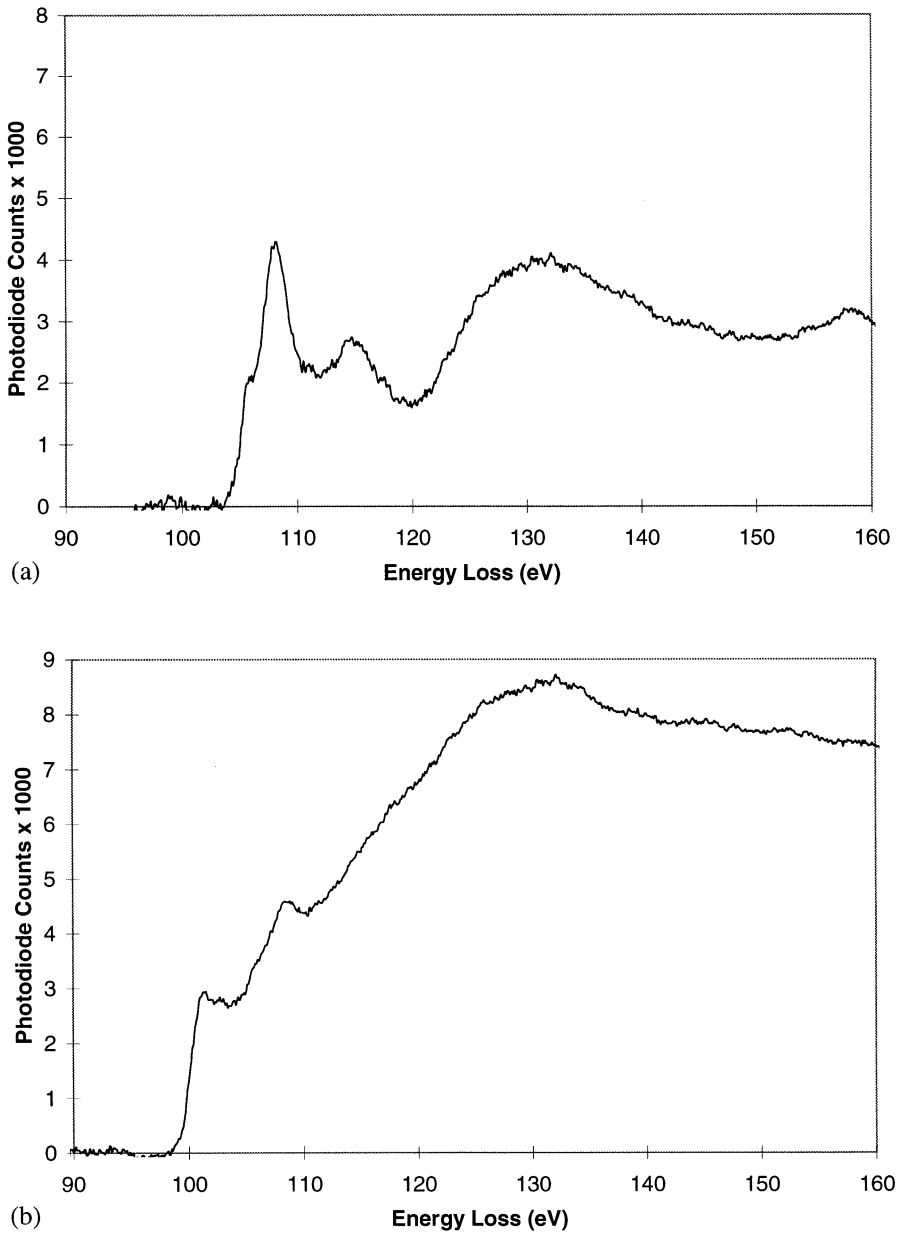

Fig. 7. Bonding configurations of Si in amorphous layer (grinding table speed 0.02 m min^{-1}): (a) upper part of the amorphous layer; and (b) lower part of the amorphous layer.

determined by the dislocation structure in the subsurface. When the table speed was low (e.g. 0.02 m min^{-1}), the dislocation penetration was shallow (100–200 nm), the dislocation density was low, no dislocation interaction took place and thus no microcracks were generated. When the speed reached 1 m min^{-1}, dislocations penetrated deeply (300–600 nm) with complex interactions. In this case, severe stress concentration occurred and microcracks appeared.

3.3. Material removal

As shown in Section 3.1 the material removal for all of the cases investigated was in the ductile mode. The mechanism of the ductile-regime grinding of silicon is therefore very different from that of the grinding of

Table 6
Grinding forces

Table speed (m min^{-1})	0.02	0.1	0.2	0.5	1
Average normal force per unit width (N mm^{-1})	0.4	0.36	0.4	0.9	1.5
Average tangential force per unit width (N mm^{-1})	0.01	0.01	0.013	0.03	0.05

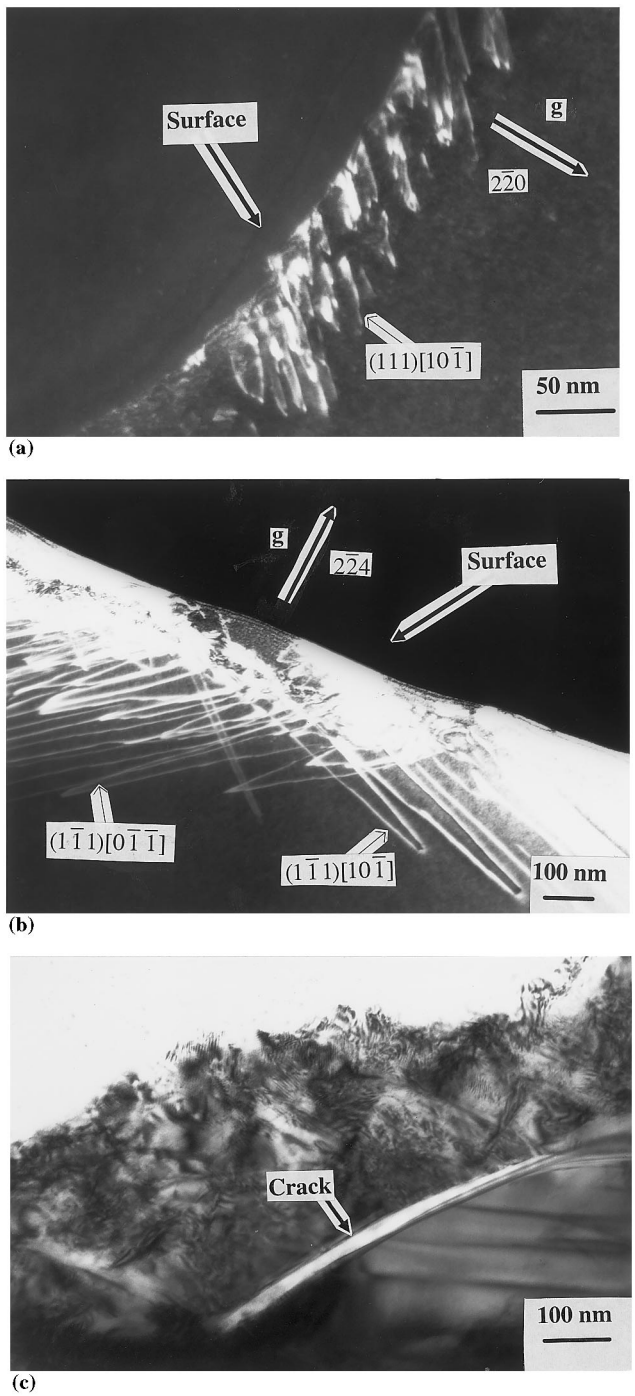

Fig. 8. Details of dislocation structures vs. table speed: (a) 0.02 m min^{-1} (note that only one dislocation system appears); (b) 1 m min^{-1} (note that two dislocation systems appear); and (c) microcracks.

alumina [8]. The ductile mode of material removal in alumina is by the initiation of a sufficient number of slip and twin systems [8]. However, this is not the case for silicon, as only up to two slip systems were initiated (Fig. 8(a) and (b)). The mechanism of the ductile mode of material removal must therefore be related to the formation of the amorphous phase. This is well supported by theoretical investigation based on molecular dynamic theory [7], which showed that amorphous phase transformation even takes place at a very small indentation depth of 1 nm.

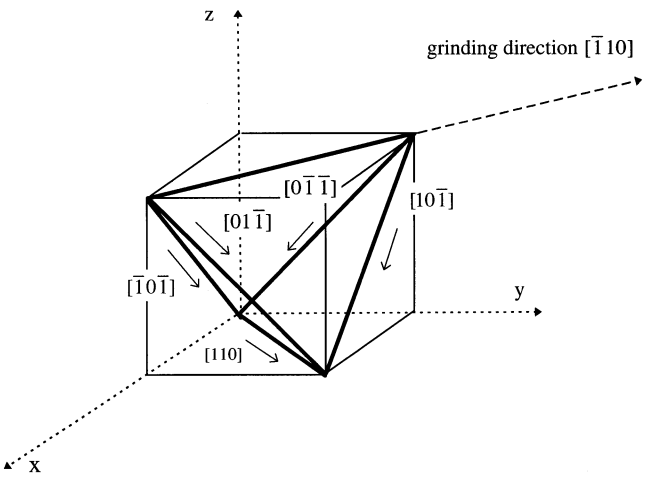

Fig. 9. Orientation of slipping planes and possible slipping directions in silicon.

4. Theoretical evaluation of dislocation penetration

For simplicity, the interaction of different slip systems is ignored in evaluating the dislocation penetration depth. This will give rise to an upper bound since dislocation interaction hinders penetration. To facilitate the analysis, it is further assumed that the force acting on the specimen surface during grinding is distributed equally between active grains and that all grains have an equal diameter of 1 μm. Based on this, the experimentally measured forces (Table 6) can be used to give the force acting on an individual grain. As the loading conditions on a grain were fixed the shear stress distribution can be determined easily [9].

Consider the slip system $\{111\}\langle 1\bar{1}0\rangle$ that is a common system in silicon, and examine all the six possible slipping directions, as shown in Fig. 9. As the grinding direction is [$\bar{1}$10] and the ground surface is (001), the dislocation movement along [$\bar{1}$10] and [110] does not affect its penetration depth. Furthermore, directions [10$\bar{1}$] and [0$\bar{1}\bar{1}$] as well as directions [$\bar{1}$01] and [01$\bar{1}$] are symmetrical to the grinding direction and thus are identical in terms of calculating the dislocation penetration depth. The shear stresses along possible slipping directions with different grinding conditions, as shown in Fig. 10, lead to the different dislocation penetration depths listed in Table 7. Similar calculations can be done for the other slip system.

Nevertheless, temperature rise alters the depth of dislocation penetration [10–12]. To examine its effect, the grinding heat is simulated using a moving heat source, as discussed in Refs. [13–17], and it is assumed that all the heat is conducted into the workpiece. Fig. 11 shows the temperature rise along the possible slipping directions.

As expected, the temperature rise significantly changes the penetration depth of dislocations. Table 7 shows that the measured penetration depth is between the predictions for with and without temperature rise effect[2]. It is understandable that the theoretical prediction with the temperature effect here is an upper bound, since not all the heat would be conducted into the workpiece in an actual grinding operation.

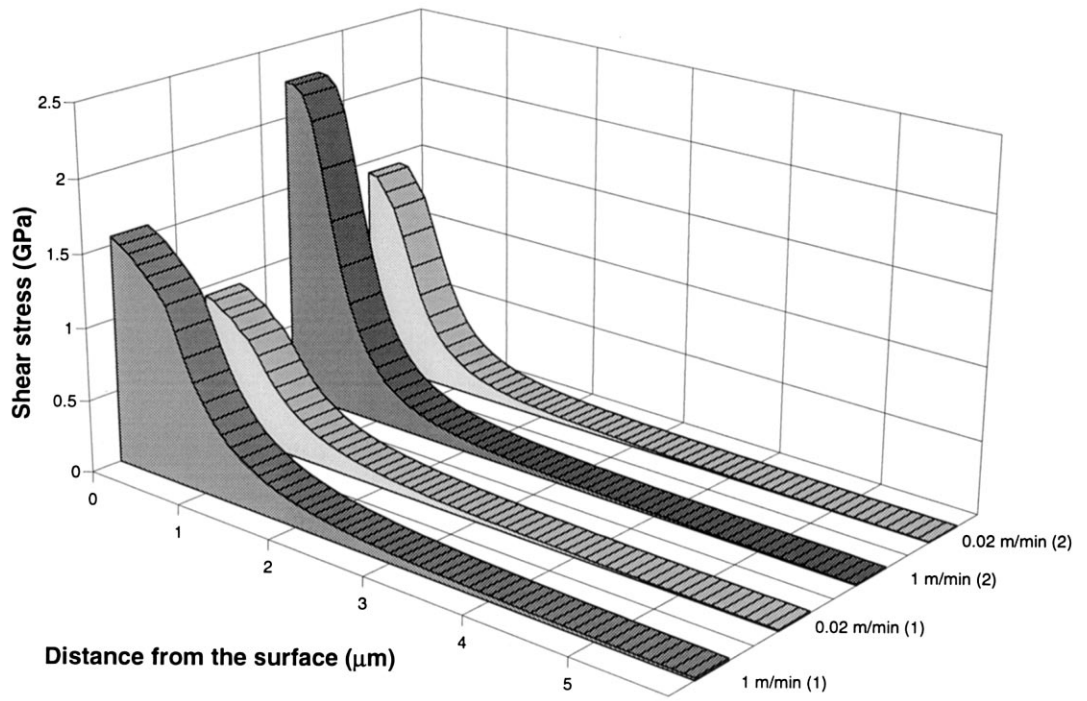

Fig. 10. Distributions of shear stresses in the subsurface along slipping directions: (1) [$\bar{1}$0$\bar{1}$] or [01$\bar{1}$]; and (2) [10$\bar{1}$] or [0$\bar{1}\bar{1}$].

Table 7
Depth of dislocation penetration

Slip systems activated	Table speed (m min^{-1})	Depth of dislocation penetration (nm)				
		Theoretical prediction				Measured
		Without temperature rise		With temperature rise		In z direction
		In sliding direction	In z direction	In sliding direction	In z direction	
$(1\bar{1}1)[10\bar{1}]$, $(111)[10\bar{1}]$, $(1\bar{1}1)[0\bar{1}\bar{1}]$, $(\bar{1}\bar{1}1)[0\bar{1}\bar{1}]$	1	400	280	1000	700	300–600
	0.02	0	0	600	420	100–200
$(\bar{1}11)[\bar{1}0\bar{1}]$, $(\bar{1}\bar{1}1)[\bar{1}0\bar{1}]$, $(\bar{1}11)[01\bar{1}]$, $(111)[01\bar{1}]$	1	0	0	900	630	300–600
	0.02	0	0	600	420	100–200

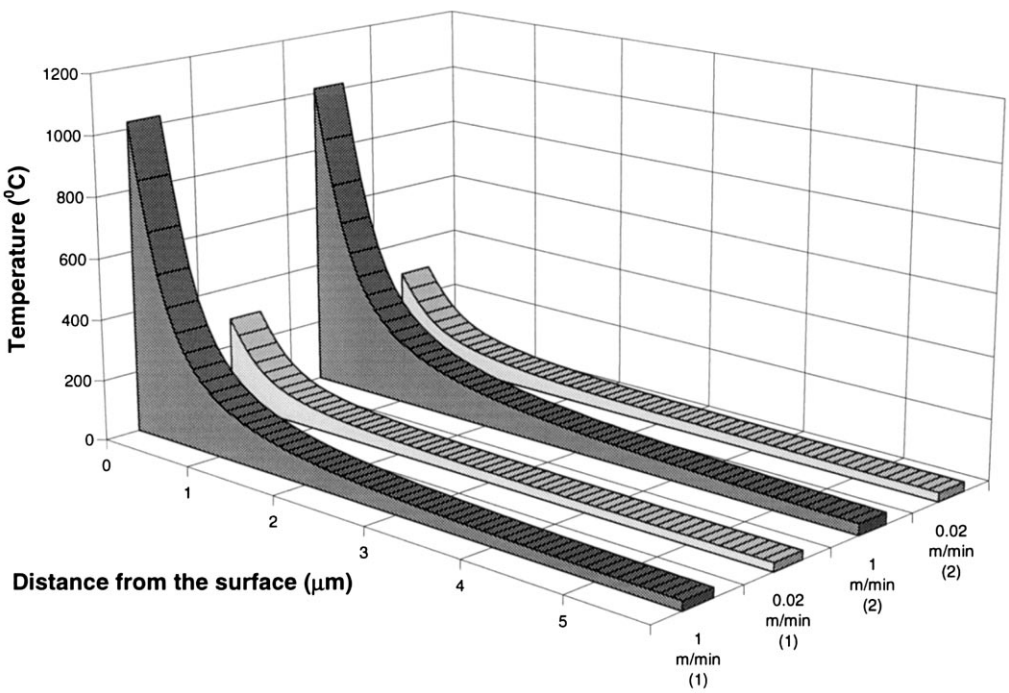

Fig. 11. Temperature rise in subsurface along slipping directions: (1) $[\bar{1}0\bar{1}]$ or $[01\bar{1}]$; (2) $[10\bar{1}]$ or $[0\bar{1}\bar{1}]$.

All of the above results indicate that the most preferable condition in the grinding of silicon monocrystals should be a low table speed, which introduces a smaller thickness of amorphous layer and a smaller depth of dislocation penetration.

5. Conclusions

1. The table speed in grinding has a very clear effect on the micro-structural change in a silicon monocrystal. It alters the total thickness of the amorphous layer, the penetration depths of oxygen, carbon and dislocations, and in turn, alters the formation of SiO_2 in the amorphous phase.

2. The mechanism of the formation of the amorphous layer is complex, but is clearly associated with the involvement of coolant and the mechanical abrasion of the cutting edges on the grinding wheel.

[2] Slipping along only two directions, $[10\bar{1}]$ and $[0\bar{1}\bar{1}]$, was possible at the high table speed (1 m min^{-1}) if no temperature rise occurred; and no dislocations were activated at low table speed (0.02 m min^{-1}). With temperature rise, slipping in all possible $<110>$ directions was activated even at low table speed (0.02 m min^{-1}).

3. The theoretical predictions of dislocation penetration are in good agreement with experimental observations. Thus the method of theoretical evaluation of dislocation penetration used here is reliable and can be used in the analysis of other ground materials.

Acknowledgements

The authors wish to thank the Australian Research Council (ARC) for continuing support of this project. We thank also the Electron Microscope Unit for the use of its facilities.

Appendix A

The notations used in the present study for slip planes and slip directions follow those specified in Ref. [18]. They are:

(001) stands for a single set of parallel planes;
{001} indicates a set of equivalent planes of this type, that is, (001), (010), etc.;
$[\bar{1}10]$ means a single direction;
$\langle\bar{1}10\rangle$ means all the directions of equivalent type, that is, [110], $[0\bar{1}\bar{1}]$, etc.

References

[1] I. Zarudi, L.C. Zhang, J. Mater. Sci. Lett. 15 (1996) 586–587.
[2] R.R. Kunz, H.R. Clark, P.M. Nitishin, M. Rotschild, B.S. Ahern, J. Mater. Res. 11 (1996) 1228–1237.
[3] S. Takayuki, F. Shigeru, M. Eiji, I. Masayuki, Prec. Eng. 18 (1996) 129–137.
[4] P.N. Blake, R.O. Scattergood, J. Am. Ceram. Soc. 73 (1990) 949–957.
[5] T.R. Mchedlidze, I. Yonenaga, K. Sumino, Mater. Sci. Forum 196–201 (1995) 1841–1846.
[6] I. Zarudi, L.C. Zhang, Y.-W. Mai, J. Mater. Sci. 31 (1996) 905–914.
[7] H. Tanaka, L.C. Zhang. Advances in Abrasive Technology, Proc. Int. Symp., 1997, (in press).
[8] I. Zarudi, L.C. Zhang, Proc. 10th ASPE (1995) 163–166.
[9] I. Zarudi, Proc. 11th ASPE (1996) 610–613.
[10] D.E. Kim, N.P. Sun, J. Mater. Sci. 28 (1993) 3895–3899.
[11] T.S. Gross, V.K. Mathews, R.J. De Angelis, K. Okazaki, Mater. Sci. Eng. 117 (1989) 75–82.
[12] V.P. Kisel, Mater. Sci. Eng. 164 (1993) 356–359.
[13] L.C. Zhang, T. Suto, H. Noguchi, T. Waida, Manufact. Rev. 5 (1992) 261–273.
[14] L.C. Zhang, T. Suto, H. Noguchi, T. Waida, in: M.H. Aliabadi, C.A. Brebbia (Eds), Computer Methods and Experimental Measurements for Surface Treatment Effects, 1993, pp. 275–284.
[15] L.C. Zhang, M. Mahdi, Int. J. Machine Tools Manufact. 35 (1995) 1397–1409.
[16] M. Mahdi, L.C. Zhang, Int. J. Machine Tools Manufact. 37 (1997) 619–633.
[17] M. Mahdi, L.C. Zhang, Comput. Struct. 56 (1995) 313–320.
[18] J.W. Edington, Typical Electron Microscope Investigation, Macmillan, London, 1976.